Passive and Active Piezoelectric Effects on Flutter Suppression of Highly Flexible Wings

Natsuki Tsushima[+1], Weihua Su[+2]
[+1, +2] University of Alabama, Tuscaloosa, AL, USA

The paper addresses both active and passive flutter suppression for highly flexible wings using piezoelectric transduction. The piezoelectric effect is included in a strain-based geometrically nonlinear beam formulation. The resulting structural dynamic equations for multifunctional beams are then coupled with a finite-state unsteady aerodynamic formulation, allowing for piezoelectric energy harvesting and actuation with the nonlinear aeroelastic system. With the development, it is possible to provide an integral aeroelastic and electromechanical solution of concurrent active piezoelectric control on and energy harvesting from wing vibrations, with the consideration of the geometrical nonlinear effects of the slender multifunctional wings. The energy harvesting system can provide an additional damping effect on the wing as well as its harvesting capability. In this paper, an LQG controller is developed for the active control of wing limit-cycle oscillations due to the onset of flutter instability. The controller demonstrates effective flutter control capability. Furthermore, a concurrent active vibration control and energy harvesting can also be realized for the multifunctional wing system with embedded piezoelectric materials.

Keyword: Flutter, Multifunctional structure, Active control, Energy harvesting, Slender wing

1. Introduction

With an increase of demands for high-performance aircraft, nonlinear aeroelasticity has been one of the most important and interested fields nowadays. With the application of flexible structures to reach the desired high performance, aeroelastic instabilities including flutter and LCOs may reduce the aircraft flight performance and lead to structural problems such as fatigue on the structures. There have been extensive literatures regarding aeroelasticity.[1] Especially, Dowell et al.[2] provided a good summary of nonlinear aeroelasticity studies, especially for flutter and limit cycle oscillations (LCOs) at the time.

High-altitude long-endurance (HALE) UAVs have been developed for several applications such as Intelligence, Surveillance, and Reconnaissance (ISR) and environmental researches. They feature high aspect-ratio slender wings with low structural weight. Due to the nature of the slender wings, they may undergo large deformations with normal operation conditions, which lead to geometrically-nonlinear behaviors.[3-5] Therefore, geometrical nonlinearity must be taken into account in the aeroelastic modeling of these vehicles.[3, 6, 7]

Recently, wing morphing has also become a dynamic research field that is hoped to improve the flight performance under different flight conditions where traditional control surfaces are less effective, or to provide extra control in poor flight conditions. Although an early concept of wing warping was employed in the aircraft system built by the Wright brothers, the technique was later replaced by discrete control surfaces due to the lack of the structural stiffness. In recent studies of the active aeroelastic wing (AAW) technology,[8] a set of control surfaces was used to induce aeroelastic deformations on the wing so that the reshape of the wing can provide optimum performance instead of directly generating the maneuver loads. The studies showed promising benefits of AAW technology in weight and performance perspectives. At the same time, multifunctional structural technologies[9] are being developed, which may bring revolutionary changes to aircraft structures. These structures are capable of performing multiple primary functions and can potentially improve aircraft performance through consolidation of subsystem materials and functions.[9, 10] The

[+1]ntsushima@crimson.ua.edu, [+2]suw@eng.ua.edu

employment of the wing morphing concept and multifunctional structural technologies may create new aircraft platforms with enhanced effectiveness and improved capability of operation.

The growth of active material technologies including anisotropic piezo-composite actuators (APA)[11] may facilitate the applications of multifunctional structures. In fact, one may take advantage of piezoelectric transducers to fulfill the dual functions of actuation and energy harvesting.[12] To explore the approaches to model the electromechanical behavior of piezoelectric transducing, many research groups from different fields have developed various prediction models. Early studies of piezoelectric transducing have modeled the piezoelectric transducer using a simplified lumped model with bending vibrations.[13] Even though the approach was effective, the lumped model came with some disadvantages, such as the over simplification of the real physics. To improve the accuracy, some distributed models have been applied in the subsequent studies. For example, Bilgen et al.[14] modeled the cantilever beam with embedded piezoelectric materials using the linear Euler-Bernoulli beam theory, and applied this approach to the piezoelectric transducing and gust alleviation of a small UAV.[15] Sodano et al.[16] developed a model of the piezoelectric power harvesting device based on works of Hagood et al.[17] and Crawley and Anderson.[18] They used energy methods to develop the constitutive equations of a bimorph piezoelectric cantilever beam. The model was solved with the Rayleigh-Ritz procedure. More recently, Anton et al.[10] presented the investigation of a multifunctional wing spar for UAVs.

On the other hand, the piezoelectric actuation was implemented for aerospace applications in many ways. For example, Bent et al.[19] developed the actuator equations for piezoelectric fiber composites with a conventional poling condition. They applied the Classical Laminated Plate Theory (CLPT) for the anisotropic composites force calculations. Wilkie et al.[20] employed this approach to find the piezoelectric induced stress and to calculate the resultant moment on a rectangular, thin-walled, closed-section structure with the piezoelectric twist actuation. Cesnik and Ortega-Morales[21] used an energy approach for the actuation equations for a composite wing. They compared their model capability with preceding studies in the literature.[22] Furthermore, an integrated structure of active actuation and energy harvesting may be designed by utilizing piezoelectric materials. Such a structure may work with one of the two functions of piezoelectric materials, which can be either actuated for wing morphing and/or vibration control, replacing the traditional control surfaces, or used as an energy harvester.

Finally, control algorithms are required to properly actuate the active wing structures to achieve the desired aircraft performance. In a modern aircraft control system, there are multiple variables that need to be controlled simultaneously. To satisfy the mission requirement and achieve the desired flight performance, an optimal feedback strategy should be implemented. In a simple control problem, Linear Quadratic Regulator (LQR) or more practical Linear Quadratic Gaussian (LQG) regulator may be selected as the starting point. These regulators are popular due to their capability to obtain the optimal control configurations. A lot of literatures[23] have provided detailed discussions on these controllers.

In summary, as a study on the aforementioned integrated system, this paper will model both active piezoelectric actuation and energy harvesting in a strain-based geometrically nonlinear aeroelastic formulation. Numerical studies will be performed to explore the concurrent piezoelectric energy harvesting and wing flutter control of the multifunctional system.

2. THEORETICAL FORMULATION

The theoretical formulation used in the current study is introduced in this section, where a slender wing with piezoelectric actuation is modeled using a strain-based geometrically-nonlinear beam formulation. The strain-based beam[24] and aeroelastic[4, 5] formulations have been introduced in the literature. The finite-state inflow theory[25] is incorporated for aerodynamic loads on lifting surfaces. Piezoelectric actuation is considered as an additional external load to the system.

(1) Multifunctional wing structure

Fig. 1 illustrates a multifunctional beam with both energy harvesting and actuation capabilities, using piezoelectric materials. The current work is an extension to the piezoelectric actuation based on the previous

work on the modeling of the piezoelectric energy harvesting.[26] For simplicity, the piezoelectric energy harvesting works in the flap bending direction.

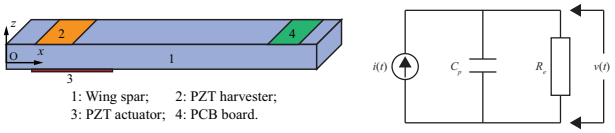

Figure 1: Multifunctional beam and equivalent circuit for energy harvesting subsystem.

The constitutive equation for piezoelectric materials is given as

$$\begin{Bmatrix} \bar{\boldsymbol{\sigma}} \\ \bar{\mathbf{B}} \end{Bmatrix} = \begin{bmatrix} \bar{\mathbf{D}} & -\mathbf{e}^{\mathrm{T}} \\ \mathbf{e} & \boldsymbol{\zeta} \end{bmatrix} \begin{Bmatrix} \bar{\boldsymbol{\varepsilon}} \\ \mathbf{E} \end{Bmatrix} \tag{1}$$

where $\bar{\boldsymbol{\sigma}}$ is the material stress, $\bar{\mathbf{B}}$ is the electric displacement, $\bar{\mathbf{D}}$ is the piezoelectric material stiffness matrix, $\mathbf{e}$ is the piezoelectric coupling, $\boldsymbol{\zeta}$ is the permittivity, $\bar{\boldsymbol{\varepsilon}}$ is the material strain, and $\mathbf{E}$ is the electric field, which is obtained from the gradient of the electric voltage v across the piezoelectric layer. The coupled electromechanical effect of piezoelectric material will be considered when deriving the equations of motion.

(2) Fundamental wing modeling description

A cantilever beam is defined in a fixed frame B. A local beam frame (w) is built within the B frame (see Fig. 2), which is used to define the position and orientation of each node along the beam reference line. Vectors $\mathbf{w_x}(s,t)$, $\mathbf{w_y}(s,t)$, and $\mathbf{w_z}(s,t)$ are bases of the beam frame w, whose directions are pointing along the beam reference axis, toward the leading edge, and normal to the beam (wing) surface, respectively, resolved in the B frame. The curvilinear beam coordinate s provides the nodal location within the body frame.

To model the elastic deformation of slender beams, a new nonlinear beam element was developed in the work of Ref. [24, 27]. Each of the elements has three nodes and four local strain degrees of freedom, which are extension, twist, flap bending rate (κ_y), and edge bending rate (κ_z), respectively, of the beam reference line:

$$\boldsymbol{\varepsilon}^T(s) = \{\varepsilon_x(s) \quad \kappa_x(s) \quad \kappa_y(s) \quad \kappa_z(s)\} \tag{2}$$

which is not to be confused with the strain of the materials ($\bar{\boldsymbol{\varepsilon}}$) in Eq. 1, even though they are related.

Positions and orientations of each node along the beam are determined by a vector consisting of 12 components, and the derivative and variation dependent variable $\mathbf{h}$ are derived from those of the independent variable $\boldsymbol{\varepsilon}$ using the Jacobians $\mathbf{J}$ which are obtained from kinematics.[6, 24]

(3) Equations of motion

The equations of motion can be derived by following the principle of virtual work. The detailed derivation, where the electromechanical coupling effect was not considered, can be found in Su and Cesnik.[4, 24] The electromechanical coupling effect was further discussed and studied for energy harvesting.[26] By putting internal and external virtual works together, the total virtual work on a beam can be obtained.[28] Because the variations of the strain and the voltage are arbitrary, the electromechanical system's equations of motion is

$$\begin{aligned} &\mathbf{M}_{\mathbf{FF}}\ddot{\boldsymbol{\varepsilon}} + \mathbf{C}_{\mathbf{FF}}\dot{\boldsymbol{\varepsilon}} + \mathbf{K}_{\mathbf{FF}}\boldsymbol{\varepsilon} = \mathbf{R}_{\mathbf{F}} \\ &\mathbf{B}_{\mathbf{vh}}^{\mathbf{T}}\boldsymbol{\varepsilon} + C_p v + Q_e = 0 \quad \text{or} \quad \mathbf{B}_{\mathbf{vh}}^{\mathbf{T}}\dot{\boldsymbol{\varepsilon}} + C_p \dot{v} + v/R_e = 0 \end{aligned} \tag{3}$$

where the generalized inertia, damping, stiffness matrices and generalized force vector are

$$\begin{aligned} &\mathbf{M}_{\mathbf{FF}}(\boldsymbol{\varepsilon}) = \mathbf{J}_{\mathbf{h}\varepsilon}^{\mathbf{T}}\mathbf{M}_{\mathbf{s}}\mathbf{J}_{\mathbf{h}\varepsilon} \qquad \mathbf{C}_{\mathbf{FF}}(\boldsymbol{\varepsilon},\dot{\boldsymbol{\varepsilon}}) = \mathbf{C}_s + \mathbf{J}_{\mathbf{h}\varepsilon}^{\mathbf{T}}\mathbf{M}_{\mathbf{s}}\dot{\mathbf{J}}_{\mathbf{h}\varepsilon} \qquad \mathbf{K}_{\mathbf{FF}} = \mathbf{K}_{\mathbf{s}} \\ &\mathbf{R}_{\mathbf{F}} = \mathbf{K}_{\mathbf{FF}}\boldsymbol{\varepsilon}_{\mathbf{0}} + \mathbf{J}_{\mathbf{h}\varepsilon}^{\mathbf{T}}\mathbf{N}\mathbf{g} + \mathbf{J}_{\mathbf{p}\varepsilon}^{\mathbf{T}}\mathbf{B}^{\mathbf{F}}\mathbf{F}^{\mathbf{dist}} + \mathbf{J}_{\mathbf{0}\varepsilon}^{\mathbf{T}}\mathbf{B}^{\mathbf{M}}\mathbf{M}^{\mathbf{dist}} + \mathbf{J}_{\mathbf{p}\varepsilon}^{\mathbf{T}}\mathbf{F}^{\mathbf{pt}} + \mathbf{J}_{\mathbf{0}\varepsilon}^{\mathbf{T}}\mathbf{M}^{\mathbf{pt}} + (\mathbf{B}_{\mathbf{va}} + \mathbf{B}_{\mathbf{vh}})v \end{aligned} \tag{4}$$

in which $\boldsymbol{\varepsilon}_{\mathbf{0}}$ is the initial strain of the beam. $\mathbf{B_{va}}$ and $\mathbf{B_{vh}}$ are the electromechanical coupling matrix for the piezoelectric actuator and harvester. $\mathbf{g}$, $\mathbf{F^{dist}}$, $\mathbf{M^{dist}}$, $\mathbf{F^{pt}}$, and $\mathbf{M^{pt}}$ are the gravity field, distributed forces, distributed moments, point forces, point moments, respectively. $\mathbf{N}$, $\mathbf{B^F}$, and $\mathbf{B^M}$ are the influence matrices for

the gravitational force, distributed forces, and distributed moments, which come from the numerical integration. In addition, Q_e is the total charge accumulated over the electrodes, whose time derivative is the current. The coupling matrix $\mathbf{B_{va}}$ will be derived in the next discussion while $\mathbf{B_{vh}}$ and C_p are from the cross-sectional value:

$$\begin{aligned} \mathbf{B_{vh}} &= [0 \quad 0 \quad B_{vh} \quad 0]^T \\ B_{vh} &= B_{vh}^{cs} s_p = s_p \int_A -\left(z_p e_{31} / t_p\right) dA \\ C_p &= \zeta b_p s_p / t_p \end{aligned} \tag{5}$$

in which A is the cross-sectional area of the piezoelectric layer. z_p is the distance between the elastic axis of the beam and the piezoelectric layer (see Fig. 3). Quantities b_p, t_p, and s_p are the width, thickness, and length of the piezoelectric layer, respectively. As shown in Eq. 4, the generalized force vector involves the effects from initial strains $\boldsymbol{\varepsilon_0}$, gravitational field $\mathbf{g}$, distributed forces $\mathbf{F^{dist}}$, distributed moments $\mathbf{M^{dist}}$, point forces $\mathbf{F^{pt}}$, point moments $\mathbf{M^{pt}}$, and the electric field v. The aerodynamic forces and moments are considered as distributed loads.

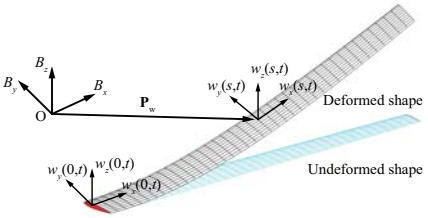

Figure 2: Beam references frames.

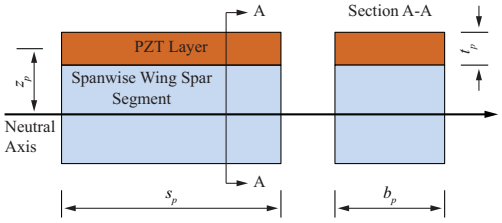

Figure 3: Spanwise segment and cross-section of multifunctional wing spar.

(4) Piezoelectric actuation of bending and torsion deformation

The multifunctional wing with embedded piezoelectric materials is also considered as a piezoelectric actuation device, in addition to the energy harvesting function. Bent et al.[19] developed the anisotropic actuator equations using the conventional poling, which are followed in the current development of the structural dynamic equations of the multifunctional wing. With the in-plane structural anisotropy in the piezoelectric material, a transformation between a piezoelectric material and beam coordinate, and the assumption of plane stress (T_3=T_4=T_5=0), the reduced piezoelectric constitutive relations are obtained.[28] The electric field and displacement are assumed to be along the 3-direction for simplicity. Piezoelectric induced stresses can be

$$\bar{\boldsymbol{\sigma}}_{\mathbf{pe}} = -\mathbf{T_s^T} \tilde{\mathbf{e}}^{\mathbf{T}} E_3 \tag{6}$$

Resultant forces and moments can be calculated from the piezoelectric induced terms. Bent et al.[19] developed the forces and moments on thin-walled anisotropic composites using the Classical Laminated Plate Theory (CLPT). The detailed discussion of the CLPT can be found in Ref. [29]. On the other hand, if a composite structure is a simple rectangular thin-walled section, one may choose an approach using the piezoelectric induced stresses to calculate the induced bending and torsional moments as in Ref. [20].

The coupling matrix $\mathbf{B_{va}}$ is related to the resultant piezoelectric forces and moments as

$$\{B_{va1} \quad B_{va2} \quad B_{va3} \quad B_{va4}\}^T v = \{F_{1a} \quad M_{1a} \quad M_{2a} \quad M_{3a}\}^T \tag{7}$$

where F_{1a} is a piezoelectric induced extensional force, and M_{1a}, M_{2a}, M_{3a} are piezoelectric induced moments about 1, 2, 3 axes, respectively. In this paper, the 1, 2, 3 axes are oriented so that the coordinate aligned with the wing beam coordinate axes *x, y, z*.

(5) Unsteady aerodynamics

The distributed loads, $\mathbf{F^{dist}}$ and $\mathbf{M^{dist}}$ in Eq. 4 are divided into aerodynamic loads and user-supplied loads. The unsteady aerodynamic loads used in the current study are based on the two dimensional (2-D) finite-state inflow theory, provided in Peters and Johnson.[25] The theory calculates aerodynamic loads on a thin

airfoil section undergoing large motions in an incompressible inviscid subsonic flow. The lift, moment, and drag of a thin 2-D airfoil section about its midchord are given by

$$\begin{aligned} l_{mc} &= \pi\rho b^2(-\ddot{z}+\dot{y}\dot{\alpha}-d\ddot{\alpha})+2\pi\rho b\dot{y}^2[-\dot{z}/\dot{y}+(b/2-d)\dot{\alpha}/\dot{y}-\lambda_0/\dot{y}] \\ m_{mc} &= 2\pi\rho b^2(-\dot{y}\dot{z}/2-d\dot{y}\dot{\alpha}/2-\dot{y}\lambda_0/2-b^2\ddot{\alpha}/16) \\ d_{mc} &= -2\pi\rho b(\dot{z}^2+d^2\dot{\alpha}^2+\lambda_0^2+2d\dot{\alpha}\dot{z}+2d\dot{\alpha}\lambda_0) \end{aligned} \tag{8}$$

where b is the semichord, and d is the distance of the mid-chord in front of the reference axis. The quantity $-\dot{z}/\dot{y}$ is the angle of attack that consists of the contribution from both the steady state angle of attack and the unsteady plunging motion of the airfoil. The different velocity components are shown in Fig. 4. The inflow velocity λ_0 accounts for induced flow due to free vorticity, which is the weighted summation of the inflow states λ as described Peters and Johnson[25] and governed by

$$\dot{\boldsymbol{\lambda}} = \mathbf{F}_1\ddot{\boldsymbol{\varepsilon}} + \mathbf{F}_2\dot{\boldsymbol{\varepsilon}} + \mathbf{F}_3\boldsymbol{\lambda} \tag{9}$$

The aerodynamic loads about the midchord center are transferred to the wing elastic axis and rotated into the fixed B frame for the solution of equations of motion.

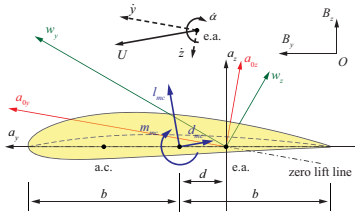

Figure 4: Airfoil coordinate system and velocity components.

(6) LQR and LQG feedback controllers

Linear Quadratic Regulator (LQR)[23] (see Fig. 5) is commonly used in traditional aircraft control studies. To apply the linear control theory, the linearization of the system equations about a nonlinear equilibrium state is performed.[28] The structural Jacobians are assumed to be constant when the system is perturbed, while this assumption holds for small perturbations to the system. It helps to simplify the linearization process by making the generalized mass matrices independent of the state variables. The nonlinear aeroelastic equations of the cantilever wing is rewritten with the small perturbation about the nonlinear equilibrium state, which yields

$$\begin{aligned} &\bar{\mathbf{M}}_{\mathbf{FF}}\ddot{\boldsymbol{\varepsilon}} + \bar{\mathbf{C}}_{\mathbf{FF}}\dot{\boldsymbol{\varepsilon}} + \bar{\mathbf{K}}_{\mathbf{FF}}\boldsymbol{\varepsilon} - \mathbf{R}^{\mathbf{aero}}_{\mathbf{F}/\lambda_0}\boldsymbol{\lambda} - \mathbf{B}_{\mathbf{v}}\mathbf{v} = \mathbf{0} \\ &\dot{\boldsymbol{\lambda}} - \mathbf{F}_1\ddot{\boldsymbol{\varepsilon}} - \mathbf{F}_2\dot{\boldsymbol{\varepsilon}} - \mathbf{F}_3\boldsymbol{\lambda} = \mathbf{0} \end{aligned} \tag{10}$$

where $\bar{\mathbf{M}}$, $\bar{\mathbf{C}}$, and $\bar{\mathbf{K}}$ are the linearized general inertia, damping, and stiffness matrices. $\mathbf{R}^{\mathbf{aero}}_{\mathbf{F}/\lambda_0}$ is the derivative of the aerodynamic load vector with respect to the inflow states. Eq. 10 is put into the state-space form:

$$\begin{aligned} &\dot{\mathbf{x}} = \mathbf{A}\mathbf{x} + \mathbf{B}\mathbf{u} \\ &\mathbf{x} = \{\boldsymbol{\varepsilon}^{\mathbf{T}} \quad \dot{\boldsymbol{\varepsilon}}^{\mathbf{T}} \quad \boldsymbol{\lambda}^{\mathbf{T}}\}^{\mathbf{T}} \qquad \mathbf{u} = \{\mathbf{v}^{\mathbf{T}}\}^{\mathbf{T}} \end{aligned} \tag{11}$$

where $\mathbf{v}$ is the inputs of piezoelectric actuation. The associated quadratic performance index is defined as

$$J = \int_0^{\infty}\left(\mathbf{x}^{\mathbf{T}}\mathbf{Q}\mathbf{x} + \mathbf{u}^{\mathbf{T}}\mathbf{R}\mathbf{u}\right)dt \tag{12}$$

where $\mathbf{R}$ and $\mathbf{Q}$ are positive-definite penalty matrices. The optimal control and associated Riccati-equation are

$$\begin{aligned} &\mathbf{u} = -\mathbf{K}\mathbf{x} \\ &\mathbf{K} = \mathbf{R}^{-1}\mathbf{B}^{\mathbf{T}}\mathbf{S} \\ &\mathbf{A}^{\mathbf{T}}\mathbf{S} + \mathbf{S}\mathbf{A} - \mathbf{S}\mathbf{B}\mathbf{R}^{-1}\mathbf{B}^{\mathbf{T}}\mathbf{S} + \mathbf{Q} = \mathbf{0} \end{aligned} \tag{13}$$

The LQR results in a robust closed-loop system. However, the LQR design assumes all the states of the system are available for feedback. In most practical systems, it is not possible to obtain all the state. The

Linear Quadratic Gaussian regulator (LQG) provides the compensation to the limitation of state variable availability. The LQG consists of an LQR and a Kalman filter which gives state estimations (see Fig. 5). The state-space model describing the problem is now

$$\begin{aligned} \dot{\mathbf{x}} &= \mathbf{A}\mathbf{x} + \mathbf{B}\mathbf{u} + \mathbf{G}\mathbf{w} \\ \mathbf{y} &= \mathbf{C}\mathbf{x} + \mathbf{D}\mathbf{u} + \mathbf{H}\mathbf{w} + \mathbf{n} \end{aligned} \tag{14}$$

where **x** is the state vector, **u** is the control input to the system plant, **w** is the process noise, and **n** is the sensor noise. The noises **w** and **n** are zero-mean white noises. The Kalman filter provides an estimated $\hat{\mathbf{x}}$ of **x** with

$$\begin{aligned} \dot{\hat{\mathbf{x}}} &= \mathbf{A}\hat{\mathbf{x}} + \mathbf{B}\mathbf{u} + \mathbf{L}(\mathbf{y} - \mathbf{C}\hat{\mathbf{x}} - \mathbf{D}\mathbf{u}) \\ \mathbf{y} &= \mathbf{C}\mathbf{x} + \mathbf{D}\mathbf{u} + \mathbf{H}\mathbf{w} + \mathbf{n} \\ \mathbf{L} &= \mathbf{P}\mathbf{C}^{\mathrm{T}}\mathbf{R}^{-1} \\ \mathbf{A}\mathbf{P} + \mathbf{P}\mathbf{A}^{\mathrm{T}} + \mathbf{Q}_{\mathbf{n}} - \mathbf{P}\mathbf{C}^{\mathrm{T}}\mathbf{R}_{\mathbf{n}}^{-1}\mathbf{C}\mathbf{P} &= \mathbf{0} \end{aligned} \tag{15}$$

where $\mathbf{Q_n}$ and $\mathbf{R_n}$ are the covariance matrices of noise **w** and **n**, and **L** is the filter gain. The control input to the original model can be obtained as

$$\mathbf{u} = -\mathbf{K}\hat{\mathbf{x}} \tag{16}$$

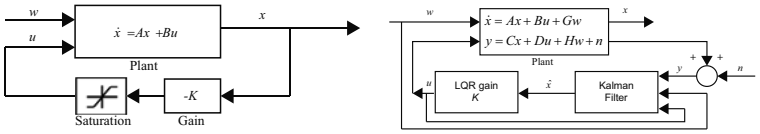

Figure 5: LQR (left) and LQG (right) feedback control diagram.

The linear quadratic controllers minimize a certain performance index by applying penalties on both state variables and control inputs. Different combinations of penalties may result in different control system performances. It may reduce the excess wing deformations with large control power, while it may allow a certain level of wing vibration, saving the excess power consumption. Therefore, it is important to establish a way to evaluate the trade-off and find a cost effective controller setting.

One good way to evaluate the performance is to normalize the cost function and to split them into two components for state variables and control inputs, which can be defined as the state cost J_s and the control cost J_c.[30] The objective cost function defined in the Eq. 12 can be rewritten with an additional weighting term r:

$$J = \int_0^\infty \left(\mathbf{x}^{\mathrm{T}}\mathbf{Q}\mathbf{x} + r\mathbf{u}^{\mathrm{T}}\mathbf{R}\mathbf{u} \right) dt \tag{17}$$

As a preliminary design, the balanced penalty point, cost effective point in other words, can be found at the vertex of the hyperbolic curve of state and control cost.[28]

3. NUMERICAL STUDIES

In this section, nonlinear active aeroelastic analysis results are presented for a slender wing, which are obtained by using the derived electro-aeroelastic formulation. Passive and active suppressions of the wing flutter are also discussed. Particularly, concurrent active piezoelectric actuation and energy harvesting with a LQG controller are explored with different multifunctional wing configurations.

(1) Multifunctional wing

The multifunctional wing model in Ref. [28] is used for the study of flutter suppression. The detailed wing properties can be found in Ref. [30]. The wing model is divided into 10 elements. Some of the elements are “designated” as active actuators for the vibration control, while others are “designated” as energy harvesters. The system resistance load is set to be 1 MΩ. Fig. 6 is the wing geometry and the lay-up of the cross-section. The model applies Active Fiber Composites (AFC) for bending twist actuation and it is tapered through 75% of the wing. There is a single wing spar at 40% chord, and element IDs are assigned from the wing root to the tip, ranging from 1 to 10. Although the studies in Ref. [30] covered different actuator

orientations from 0˚ to ±45˚, only the case with the actuation oriented at ±22˚ is performed in the current study to have the balanced bending and torsional actuation capability.

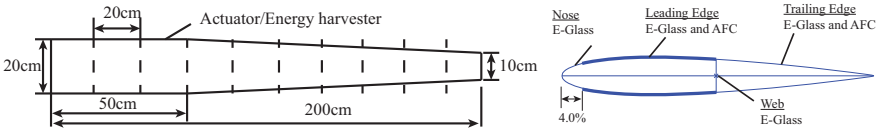

Figure 6: Wing model dimensions and lay-up of the cross-section.

(2) Stability analysis and flutter boundary

A stability analysis[4] is performed to properly understand the wing aeroelastic stability characteristics. To evaluate the impacts of gravity and angle of attack (AOA) α on the flutter boundary of the wing, several conditions with and without a gravity load at different AOAs are investigated as shown in Fig. 7. The flutter speed U_F and the frequency ω_F depend on the AOA, but the gravity effect seems to be negligible for the wing and it will not be considered in the following analysis for simplicity. To consider a specific case for flutter, α = 8° is chosen, and the flight altitude is set as sea level in the following studies. The stability analysis yields U_F = 71.4 m/s and ω_F = 22.3 Hz. The flutter behavior of the wing with the condition is then simulated in the time-domain. Fig. 8 shows the wing tip vertical deflection at U_∞ = 89.25 m/s which is 25% above the flutter speed, which will be used in the following flutter control studies.

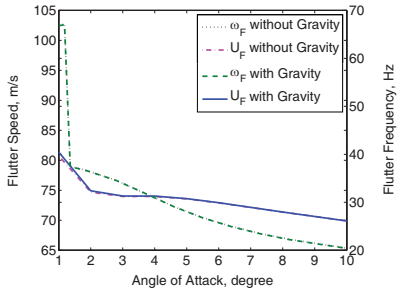

Figure 7: Flutter speed and frequency.

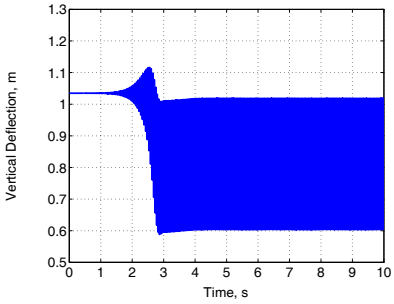

Figure 8: Wing tip vertical deflection at U_∞ = 89.25 m/s and α = 8°.

(3) Passive damping with energy harvesting

Energy harvesting has an additional damping effect,[26] so called shunt damping, associated to its harvesting function, which is studied in this section. To focus on the damping effect due to the energy harvesting, all the multifunctional wing elements are activated as harvesters in this section. Fig. 9 shows the wing tip vertical deflections of two aeroelastically neutral cases, while impacted by the energy harvesting subsystem. In the first one α = 2° and U_∞ = 76 m/s, while the second has α = 8° and U_∞ = 73.75 m/s. Since the passive damping magnitude from this system is not so large, it cannot provide a large flutter suppression effect all the time. However, it can suppress the small vibration as can be seen in the first case.

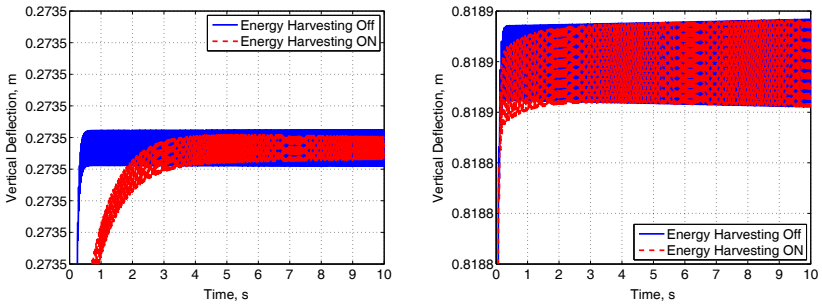

Figure 9: Wing tip vertical deflection at α = 2° and U_∞ = 76 m/s (left), α = 8° and U_∞ = 73.75 m/s (right) with and without energy harvesting.

(4) Active control analysis

A LQG controller is then investigated for flutter control. Because the LQG estimates the states through the Kalman filter, the filter setting is very important for the feedback control design. The Kalman filter is configured based on the flight condition at U_∞ = 89.25 m/s. Even though the controller will not be fully optimized, the filter is designed to give the feasible estimation (Fig. 10) for an effective control of the wing. The controller setting is chosen based on the result in Ref. [28]. To suppress the flutter, wing vibrations should be constrained. Therefore, a strong vibration penalty is used in this analysis by using a higher weighting term r. Fig. 11 shows the vertical wing tip deflection without and with LQG controller. It can be seen that the LQG provides a very good stability control when the flow speed is above the flutter boundary.

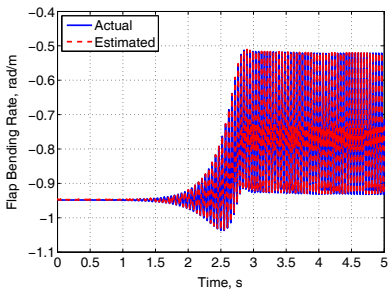

Figure 10: Estimated and actual flap bending rate.

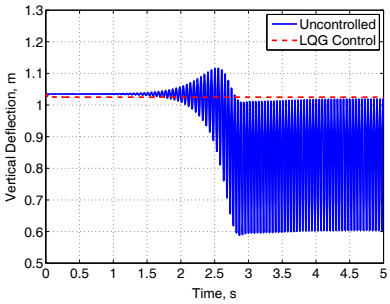

Figure 11: Wing tip vertical deflection at U_∞ = 89.25 m/s and α = 8° without and with LQG.

(5) Concurrent active control and energy harvesting system

A parametric study of concurrent active control and energy harvesting is performed in this section. Based on the vibration mode, positions closer to the wing root have higher bending rates. Thus, it is more efficient to place controllers closer to the wing root for the flutter control. The rest of the elements can be used as energy harvesters to scavenge some energy. Starting with the multifunctional configuration in which all the wing element are designated as actuator, various configurations are tested as shown in Tab. 1. Fig. 12 shows the wing tip vertical deflection with each multifunctional configuration. Cases 5 and 6 have a limit cycle oscillation with 1 cm and 0.5 cm, respectively. Cases 7 to 9 settle back to an almost stable deflection, but Case 10 cannot provide any flutter control capability. Tab. 2 lists the output and input voltages from each harvester and actuator in the different configurations. Cases 5 to 7 can provide a certain amount of harvesting energy while controlling flutter with small vibration allowed. Cases 8 and 9 show an excellent flutter control effectiveness with some harvesting outputs. The result is due to the combination of active control of actuator and passive damping from harvester.

Table 1: Multifunctional wing configurations for each simulation case.

Simulation case	1	2	3	4	5	6	7	8	9	10
Actuator element ID	1 – 10	1 – 9	1 – 8	1 - 7	1 – 6	1 - 5	1 – 4	1 - 3	1 - 2	1
Harvester element ID	-	10	9 – 10	8 - 10	7 – 10	6 - 10	5 – 10	4 - 10	3 - 10	2 - 10

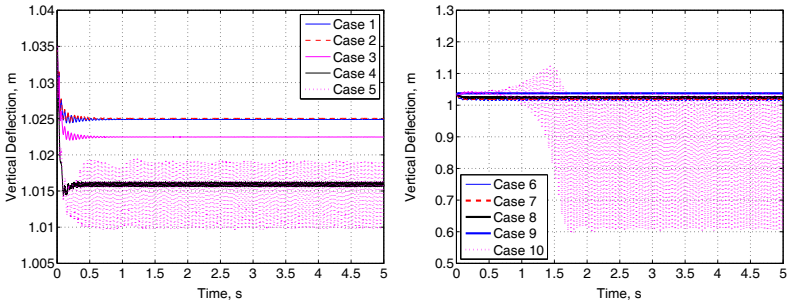

Figure 12: Wing tip vertical deflection at U_∞ = 89.25 m/s with each multifunctional configuration.

Table 2: Root mean square voltage output/input (V_{rms}, V) with typical wing cases.

Case	V_{rms}, V	Element ID (from root)										Total
		1	2	3	4	5	6	7	8	9	10	
1	Harvest output	-	-	-	-	-	-	-	-	-	-	-
	Actuation input	1318.9	480.6	1497.7	1997.9	1998.4	1998.8	1998.9	1849.5	753.2	29.2	13922.9
5	Harvest output	-	-	-	-	-	-	6.226	6.310	5.562	6.132	24.230
	Actuation input	1614.6	1973.1	1999.4	1999.4	1999.4	1999.2	-	-	-	-	11585.1
9	Harvest output	-	-	1.211	0.932	0.811	0.767	0.683	0.555	0.365	0.156	5.479
	Actuation input	1724.3	1180.0	-	-	-	-	-	-	-	-	2904.2
10	Harvest output	-	261.075	186.858	189.158	203.085	209.275	180.086	132.267	83.701	31.251	1476.745
	Actuation input	1999.1	-	-	-	-	-	-	-	-	-	1999.1

4. CONCLUSION

An approach for studying the flutter suppression using the active and passive piezoelectric effects was introduced in the paper. The strain-based geometrically nonlinear beam formulation, which makes no approximation to the deformation of beam reference line, was coupled with electromechanical model of the piezoelectric effect. For aeroelastic analysis, the finite-state unsteady subsonic aerodynamic loads are coupled to the wing surface. The coupled electro-aeroelastic model enables the prediction of the transient electric outputs and the mechanical deformations of the electro-aeroelastic system. The nonlinear electro-aeroelastic formulation is suitable for both the active piezoelectric actuation and energy harvesting studies for highly flexible wings. Based on the formulation, a LQG controller was applied to regulate piezoelectric actuation.

A multifunctional wing having bending/torsional actuation capability was considered for active control and energy harvesting with flutter. Flutter characteristics of the wing were investigated, and it yielded U_F = 71.4 m/s and ω_F = 22.3 Hz at $\alpha = 8°$. Time-domain simulations proved the frequency-domain stability analysis results and also provided actual temporal wing behavior. The shunt damping effects from energy harvesting function on the flutter was then investigated. The energy harvesting could provide an additional passive damping effect and was helpful to achieve the aeroelastic stability in some case, yet not being very efficient. A LQG controller was also designed by setting to have the cost-effective control of vibration, allowing for the active flutter suppression. The designed controller showed good flutter control capability.

Finally, the concurrent active piezoelectric actuation control and energy harvesting were studied for the multifunctional wing. Several device placements of the multifunctional wing were tested to perform parametric study of multifunctional system performance on flutter. Most of the dual-functional wings provided its flutter control capability, while one of them could not suppress the flutter. The interesting point was that it showed that, for efficient flutter suppression, the multifunctional wing could be designed with a combination of the active control and passive piezoelectric damping. They also successively scavenged energy from the controlled vibration, which would otherwise be wasted without the energy harvesting subsystem.

REFERENCES

1) Bisplinghoff, R. L., Ashley, H., and Halfman, R. L.: Aeroelasticity, Boston, MA, Addison-Wesley, 1955.
2) Dowell, E., Edwards, J., and Strganac, T.: Nonlinear aeroelasticity, *Journal of Aircraft,* Vol. 40, No. 5, pp. 857-874, 2003.
3) Patil, M. J., Hodges, D. H., and Cesnik, C. E. S.: Nonlinear Aeroelasticity and Flight Dynamics of High-Altitude Long-Endurance Aircraft, *Journal of Aircraft,* Vol. 38, No. 1, pp. 88-94, 2001.
4) Su, W., and Cesnik, C. E. S.: Nonlinear Aeroelasticity of a Very Flexible Blended-Wing-Body Aircraft, *Journal of Aircraft,* Vol. 47, No. 5, pp. 1539-1553, 2010.
5) Su, W., and Cesnik, C. E. S.: Dynamic Response of Highly Flexible Flying Wings, *AIAA Journal,* Vol. 49, No. 2, pp. 324-339, 2011.
6) Cesnik, C. E. S., and Brown, E. L.: Modeling of High Aspect Ratio Active Flexible Wings for Roll Control, *43rd AIAA/ASME/ASCE/AHS Structures, Structural Dynamics, and Materials Conferences*. AIAA Paper 2002-1719, Denver, CO, 2002.
7) Chang, C.-S., Hodges, D. H., and Patil, M. J.: Flight Dynamics of Highly Flexible Aircraft, *Journal of*

Aircraft, Vol. 45, No. 2, pp. 538-545, 2008.
8) Pendleton, E., Flick, P., Paul, D., Voracek, D. F., Reichenbach, E., and Griffin, K.: The X-53 A Summary of the Active Aeroelastic Wing Flight Research Program, *48th AIAA/ASME/ASCE/AHS/ ASC Structures, Structural Dynamics and Materials Conference and Exhibit*. AIAA Paper 2007-1855, Honolulu, Hawaii, Apr. 23-26, 2007.
9) Christodoulou, L., and Venables, J. D.: Multifunctional Material Systems: The First Generation, *Journal of the Minerals Metals & Materials Society,* Vol. 55, No. 12, pp. 39-45, 2003.
10) Anton, S. R., Erturk, A., and Inman, D. J.: Multifunctional Unmanned Aerial Vehicle Wing Spar for Low-Power Generation and Storage, *Journal of Aircraft,* Vol. 49, No. 1, pp. 292-301, 2012.
11) Williams, R. B., Park, G., Inman, D. J., and Wilkie, W. K.: An Overview of Composite Actuators with Piezoceramic Fibers, *20th International Modal Analysis Conference*. Vol. 4753, Los Angeles, CA, pp. 421-427, Feb. 4–7, 2002.
12) Erturk, A., and Inman, D. J.: Piezoelectric Energy Harvesting, Hoboken, NJ, John Wiley & Sons, 2011.
13) Roundy, S., and Wright, P. K.: A Piezoelectric Vibration Based Generator for Wireless Electronics, *Smart Materials and Structures,* Vol. 13, No. 5, pp. 1131-1142, 2004.
14) Bilgen, O., Wang, Y., and Inman, D. J.: Electromechanical Comparison of Cantilevered Beams with Multifunctional Piezoceramic Devices, *Mechanical Systems and Signal Processing,* Vol. 27, No. 1, pp. 763-777, 2012.
15) Wang, Y., and Inman, D. J.: Simultaneous energy harvesting and gust alleviation for a multifunctional composite wing spar using reduced energy control via piezoceramics, *Journal of Composite Materials,* Vol. 47, No. 1, pp. 125-146, 2013.
16) Sodano, H. A., Park, G., and Inman, D. J.: Estimation of Electric Charge Output for Piezoelectric Energy Harvesting, *Strain,* Vol. 40, No. 2, pp. 49-58, 2004.
17) Hagood, N. W., Chung, W. H., and von Flotow, A.: Modelling of Piezoelectric Actuator Dynamics for Active Structural Control, *Journal of Intelligent Material Systems and Structures,* Vol. 1, No. 3, pp. 327-354, 1990.
18) Crawley, E. F., and Anderson, E. H.: Detailed Models of Piezoceramic Actuation of Beams, *Journal of Intelligent Material Systems and Structures,* Vol. 1, No. 1, pp. 4-25, 1990.
19) Bent, A. A., Hagood, N. W., and Rodgers, J. P.: Anisotropic Actuation with Piezoelectric Fiber Composites, *Journal of Intelligent Material Systems and Structures,* Vol. 6, No. 3, pp. 338-349, 1995.
20) Wilkie, W. K., Belvin, W. K., and Park, K. C.: Aeroelastic Analysis of Helicopter Rotor Blades Incorporating Anisotropic Piezoelectric Twist Actuation, *ASME 1996 World Congress and Exposition*. Vol. 52, pp. 423-434, 1996.
21) Cesnik, C. E. S., and Ortega-Morales, M.: Active Beam Cross-sectional Modeling, *Journal of Intelligent Material Systems and Structures,* Vol. 12, No. 7, pp. 483-496, 2001.
22) Du Plessis, A. J.: Modeling and Experimental Testing of Twist Actuated Single Cell Composite Beams for Helicopter Blade Control. M.S. thesis, Massachusetts Institute of Technology, Cambridge, MA, 1996.
23) Lewis, F. L., and Syrmos, V. L.: Optimal Control, New York, NY, John Wiley & Sons, 1995.
24) Su, W., and Cesnik, C. E. S.: Strain-Based Geometrically Nonlinear Beam Formulation for Modeling Very Flexible Aircraft, *International Journal of Solids and Structures,* Vol. 48, No. 16-17, pp. 2349-2360, 2011.
25) Peters, D. A., and Johnson, M. J.: Finite-State Airloads for Deformable Airfoils on Fixed and Rotating Wings, *Symposium on Aeroelasticity and Fluid Structure Interaction Problems, ASME Winter Annual Meeting*. Vol. 44, New York, NY, pp. 1-28, 1994.
26) Tsushima, N., and Su, W.: Modeling of Highly Flexible Multifunctional Wings for Energy Harvesting, *Journal of Aircraft*, In Press.
27) Cesnik, C. E. S., and Brown, E. L.: Active Warping Control of a Joined-Wing Airplane Configuration, *44th AIAA/ASME/ASCE/AHS/ASC Structures, Structural Dynamics, and Material Conference*. Norfolk, VA, Apr. 7-10, 2003.
28) Tsushima, N., and Su, W.: Concurrent Active Piezoelectric Control and Energy Harvesting of Highly Flexible Multifunctional Wings, *Journal of Aircraft*, Under Review.
29) Jones, R. M.: Mechanics of Composite Materials, New York, NY, McGraw-Hill, 1975.
30) Ortega-Morales, M.: Modeling and Control of the Aeroelastic Response of Highly Flexible Active Wings. Ph.D. Thesis, Massachusetts Institute of Technology, Cambridge, MA, 2000.